Article

Thermodynamic Optimization of Trigeneration Power System

Ladislao Eduardo Méndez-Cruz [1], **Miguel-Ángel Gutiérrez-Limón** [2]🆔, **Raúl Lugo-Leyte** [3]🆔
and Mauricio Sales-Cruz [1,*]🆔

[1] Departamento de Procesos y Tecnología, Universidad Autónoma Metropolitana—Cuajimalpa, Av. Vasco de Quiroga No. 4871, Colonia Santa Fé, Cuajimalpa, Mexico City 05348, Mexico; ladislao.mendez@cua.uam.mx

[2] Departamento de Energía, Universidad Autónoma Metropolitana—Azcapotzalco, Av. San Pablo No. 180, Colonia Reynosa Tamaulipas, Azcapotzalco, Mexico City 02200, Mexico; magl@azc.uam.mx

[3] Departamento de Ingeniería de Procesos e Hidráulica, Universidad Autónoma Metropolitana—Iztapalapa, Av. Ferrocarril San Rafael Atlixco No. 186, Colonia Leyes de Reforma 1ª Sección, Iztapalapa, Mexico City 09340, Mexico; lulr@xanum.uam.mx

* Correspondence: asales@cua.uam.mx

Abstract: Worldwide, the growing demand for energy has been largely met through power cycles utilizing fossil fuels. Combined cycles, which integrate a gas turbine with a steam cycle, prove to be the best alternative due to their power generation capacity and high efficiencies. This efficiency is primarily attributed to the ability to harness exhaust gases to generate steam in the heat recovery boiler, allowing additional power generation through the steam turbine. Currently, there is a quest for the integration of low-temperature power cycles to maximize the utilization of residual thermal energy flows for power generation. Therefore, this work conducts an exergetic optimization of a power trigeneration system aimed at maximizing exergetic efficiency. This system includes a gas turbine and a steam cycle coupled with three different configurations of the Organic Rankine Cycle (ORC): a simple ORC, a supercritical ORC, and an ultracritical ORC. The ORC configurations are analyzed using eight organic working fluids, namely R1234yf, R290, R134a, R1234ze, R152a, R600a, R245fa, and R123. The results show that the maximum exergetic efficiency is achieved by using R152a in the ultracritical ORC configuration coupled with the combined cycle, achieving an exergetic efficiency of 55.79%. Furthermore, the maximum power generated is attained by the steam cycle with 85,600.63 kW and 3101.21 kW for the ultracritical ORC.

Keywords: thermodynamic analysis; power output; exergetic efficiency; thermodynamic optimization; organic Rankine cycle

1. Introduction

Currently, the increasing demand for electricity generation, coupled with the ongoing reduction of natural resources, has led to both a rise in their costs and environmental degradation. Gas turbines, thermal power plants, coal-fired power plants, and combined-cycle plants are the primary technologies employed to meet this energy demand. A significant portion of total electrical power is generated using fossil fuels, particularly natural gas. Combined-cycle plants are particularly attractive due to their high thermal efficiencies and power outputs. This is achieved by harnessing exhaust gases from the gas turbine through a heat recovery boiler to generate steam, which then expands in a steam turbine to produce additional power [1,2]. The gases emitted from the heat recovery boiler chimney are released into the environment at temperatures below 180 °C. Organic Rankine Cycles (ORCs) are known for their versatility in utilizing low-temperature residual thermal energy sources for power generation. Therefore, coupling an ORC with a combined-cycle plant enhances the utilization of natural resources for power generation, leading to a reduced environmental impact reflected in lower exhaust gas temperatures [3]. Thermodynamic analysis of ORC configurations involves selecting organic fluids based on criteria such as

performance, safety, low environmental impact (including a low Global Warming Potential (GWP) and zero Ozone Depletion Potential (ODP)), and technological factors. These technological factors are analyzed from energetic, exergetic, and economic perspectives, while considering operational parameters such as evaporator pressure, turbine inlet temperature, Pinch Point temperature difference (PP), mass flow rate, thermal efficiency, power output, exergetic efficiency, flammability index, and human toxicity index [4–8].

Braimakis et al. [9] conducted an energy optimization study comparing the maximum thermal efficiencies of three regenerative ORC configurations with a simple ORC, using seven organic fluids known for their low GWP and ODP. They found regenerative ORC configurations to achieve higher thermal efficiencies of up to 20.9%, while the simple ORC had the lowest thermal efficiency of 18.02%. Kajurek et al. [6] optimized a simple ORC to identify the organic fluid from a set of ten fluids, maximizing both thermal efficiency and power generation. Wang et al. [10] maximized the power generation and thermal efficiency of an ORC using three different organic fluids with a 150 °C heat source, finding R600a to yield the highest power generation and thermal efficiency. Mustapić et al. [11] conducted an analysis and optimization of power generation involving four robust ORC configurations and a simple ORC. They utilized seven different organic fluids and a geothermal heat source ranging in temperature from 120 °C to 180 °C. The optimization model's decision variables included the temperature difference of PP, the pressure and temperature of live steam, and the condensation temperature. The findings indicated that at low thermal source temperatures, the robust ORC configurations yielded the highest power outputs. Conversely, at higher thermal source temperatures, both the simple ORC and certain robust configurations demonstrated the potential for high power generation. Furthermore, research has shown the coupling of ORC configurations with power generation systems, particularly with regard to combined cycles, to maximize heat recovery. Mohammadi et al. [12] performed a multi-objective optimization analysis on a combined cycle system comprising a gas turbine and a steam cycle integrated with a regenerative ORC, utilizing benzene as the working fluid in the latter. The primary objective of the study was to identify optimal operational conditions that would concurrently enhance exergetic efficiency and minimize the cost associated with the useful product of the system. The decision variables in the model encompassed parameters such as the inlet pressure and temperature of the steam turbine, the turbine pressure of the ORC, and the temperature differential of the preheater, among others. The findings revealed that the system's optimal operating point prioritizes cost reduction while maintaining exergetic efficiency marginally lower than its theoretical maximum. Braimakis and Karellas [13] optimized a two-stage ORC to maximize exergetic efficiency, analyzing seven organic fluids at high and low temperature stages with a residual heat source varying from 100 °C to 300 °C. Küçük and Kılıç [14] performed an exergoeconomic analysis followed by multi-objective optimization of four different ORC configurations, determining factors influencing performance parameters such as thermal efficiency, exergetic efficiency, total investment cost, and unit electricity production cost to be evaporation temperature, turbine efficiency, organic working fluid, subcooling, pump efficiency, and superheating, respectively. Sohrabi et al. compared four ORC configurations using a zeotropic mixture of pentane and hexane as the organic working fluid. The configurations analyzed were a simple ORC and a double-pressure ORC, both with and without a heat exchanger (HE). These configurations were optimized to generate the highest power output. The results showed that the double-pressure ORC with HE turned out to be the one with the highest thermal efficiency, as well as the highest exergetic efficiency [15]. Javanshir et al. analyzed a system comprising a refrigeration cycle and a simple ORC with a HE. Geothermal water served as the low-temperature heat source, and the working fluids considered were R134a, R22, and R143a. The results showed that when using R134a as the working fluid, the system exhibited the lowest thermal and exergetic efficiency, whereas, with the use of R143a, the system achieved the highest efficiencies [16].

In this work, exergetic optimization is conducted to determine the operating conditions for maximizing the exergetic efficiency of a power trigeneration system, which comprises power generation using a gas turbine, a steam cycle, and the integration of three different ORC configurations. The rationale behind this analysis lies in the fact that gas turbines and steam turbines are the primary equipment used for power generation, generating significant amounts of residual thermal energy that can be harnessed through the integration of low-temperature power cycles, primarily ORC. The three proposed ORC configurations to be analyzed in this study are simple ORC (*S-ORC*), supercritical ORC (*SP-ORC*), and ultracritical ORC (*UC-ORC*). These configurations aim to evaluate performance both in the subcritical and supercritical regions of organic fluids R1234yf, R290, R134a, R1234ze, R152a, R600a, R245fa, and R123. The selection of these organic fluids for ORC configurations depends on their critical point conditions (mainly critical temperature), having a low GWP and zero ODP.

2. Methodology

2.1. Case Study

Figure 1 illustrates the power trigeneration system comprising a gas turbine, a steam cycle, and an ORC. In the high-temperature cycle (gas turbine cycle), ambient air is compressed by the compressor to the required pressure for combustion in the combustion chamber. Compressed air is then mixed with a fuel flow in the combustion chamber to undergo combustion, resulting in a flow of combustion gases at the pressure and temperature inlet turbine (TIT). These combustion gases expand in the gas turbine to generate mechanical power, which is distributed to drive the compressor and generate electrical power for the gas turbine cycle via the electric generator. Subsequently, exhaust gases from the gas turbine are utilized to generate a steam flow through heat transfer in the heat recovery steam generator (HRSG) of the steam cycle. The superheated steam flow, at the live steam pressure and temperature, expands in the steam turbine to the condensation pressure, generating additional electrical power. The steam flow exiting the turbine condenses, releasing heat in the condenser to pump the condensed water to live steam pressure conditions. The exhaust gases exiting the HRSG of the steam cycle are considered a type of low-temperature residual heat source, which is utilized for power generation via an ORC before being discharged into the environment. Figure 1 shows three types of ORC configurations: (a) *S-ORC*; (b) *SP-ORC*; (c) *UC-ORC*. The *S-ORC* operates under the same principle as the steam cycle since it has the same components; however, the working fluid used for energy generation is an organic fluid primarily due to the conditions of low temperature and critical pressure. The *S-ORC* operates in a subcritical manner, where the live steam pressure, P_{o1}, is lower than the critical pressure of the working fluid, while the condenser operating pressure depends on ambient temperature conditions. On the other hand, there are ORC configurations operating in supercritical and ultra-supercritical modes, where live steam and reheating pressures are higher than the critical pressure of the organic fluid. The heat recovery boiler of the *SP-ORC* and *UC-ORC* only requires an EC and SH connected by a header to generate live steam flow, as the phase change from compressed liquid to superheated vapor occurs instantly, thus eliminating the need for an evaporator. The *UC-ORC* configuration integrates a reheater (REH) into the heat recovery boiler, a high-pressure turbine (HPT), and a low-pressure turbine (LPT) to evaluate the increase in power generation.
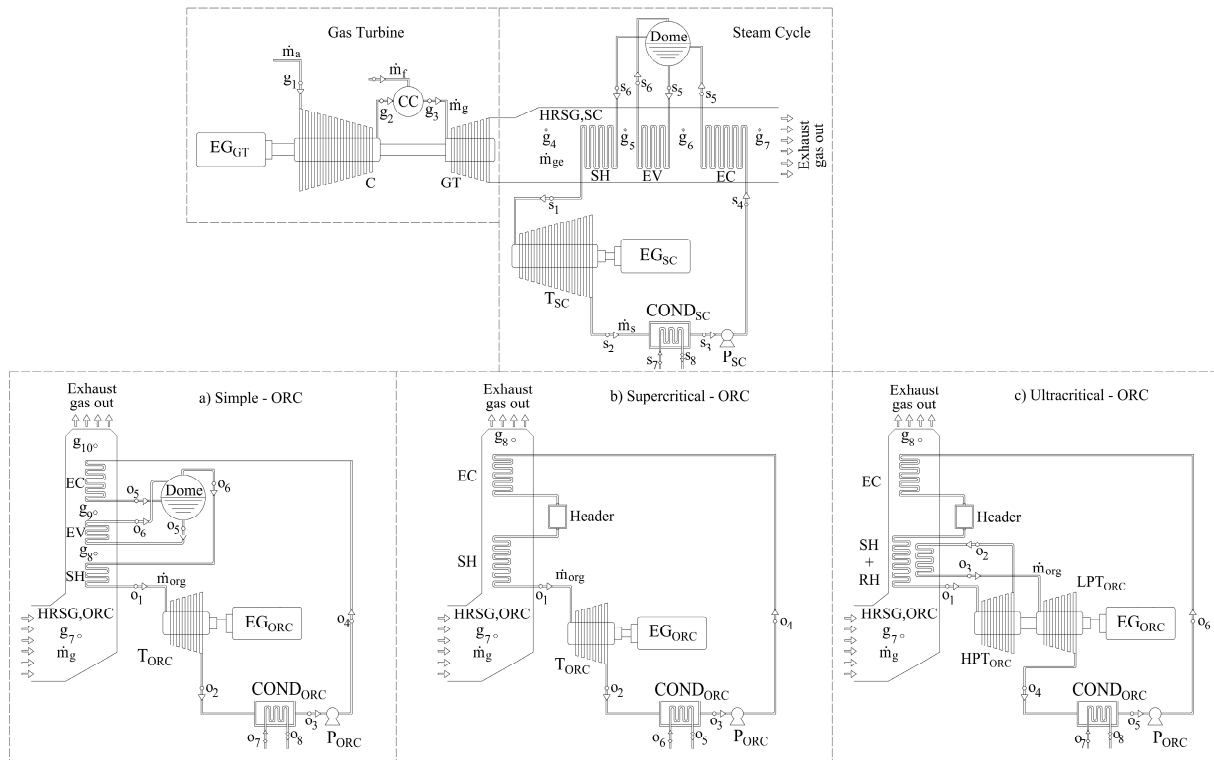
Figure 1. GT—SC power trigeneration system with the following: (**a**) *S-ORC*; (**b**) *SP-ORC*; (**c**) *UC-ORC*.

2.2. Considerations of the Case Study

The mass and energy balances of the power trigeneration system are conducted under the following considerations:

1. The gas turbine cycle, steam cycle, and ORC operate under steady-state conditions.
2. Pressure drops are only considered in the processes of the gas turbine cycle.
3. The air and fuel in the gas turbine cycle are considered perfect gases.
4. The composition of natural gas is CH_4 (88%), C_2H_6 (10%), and C_3H_8 (2%).
5. The thermodynamic properties of combustion gases include a specific heat at constant pressure, c_{pg}, of 1.289 kJ/kg K, an adiabatic index, γ_g, of 1.293, and the specific gas constant of combustion gases, R_g, of 0.29182 kJ/kg K.
6. The Low Heating Value (LHV) of the fuel is 49,514 kJ/kg_{fuel}.
7. Thermodynamic properties of water and organic fluids are estimated using REFPROP 9.1 software.
8. The hot approach temperature difference of the steam and ORC cycles is defined by $\Delta T_{HA,SH} = T_{g1} - T_{s1}$ and $\Delta T_{HA,ORC} = T_{g7} - T_{o1}$.
9. Isoentropic efficiencies of the compressor, gas turbine, steam turbine, ORC turbine, and pumps of the steam and ORC cycles are constant.
10. Changes in kinetic and potential energy in equipment processes are negligible.
11. The reference state pressure and temperature are P_0 = 1.013 bar and T_0 = 25 °C, respectively.

The thermodynamic analysis begins with an energy analysis conducted for each thermodynamic cycle of the gas turbine, steam cycle, and ORC. Energy expressions required to determine the performance parameters described earlier are developed in the energy analysis. Subsequently, an exergetic analysis is performed to evaluate the flow of irreversibilities in each component through an exergy balance. Additionally, the exergetic efficiency is determined for each power cycle, along with the overall exergetic efficiency of the power trigeneration system.

2.3. Energy Analysis

2.3.1. Gas Turbine

The airflow, $\dot{m}_a$, required to generate a given power, as a function of the fuel-to-air ratio, *far*, the ratio between the maximum and minimum temperatures, $y = T_{g3}/T_{g1}$, the isentropic efficiency of the gas turbine, η_{ITG}, the isentropic efficiency of the compressor, η_{IC}, the compressor pressure ratio, π_C, and the pressure drops in the combustion chamber, ΔP_{CC}, and in the gas turbine, ΔP_{GT}, is

$$\dot{m}_a = \frac{\dot{W}_{m,GT}}{c_{p_a}T_{g1}\left\{(1+far)\frac{c_{p_g}}{c_{p_a}}y\eta_{ITG}\left[1-\frac{(1+\Delta P_{GT})^{x_g}}{[\pi_C(1-\Delta P_{CC})]^{x_g}}\right]-\frac{1}{\eta_{IC}}\left(\pi_C^{x_a}-1\right)\right\}} \tag{1}$$

The heat supplied, $q_{sup,CC}$, into the combustion chamber per unit mass is

$$q_{sup,CC} = c_{p_a}T_{g1}\left[(1+rca)\frac{c_{p_g}}{c_{p_a}}y-1-\left(\frac{\pi_C^{x_a}-1}{\eta_{IC}}\right)\right] \tag{2}$$

The fuel flow rate, $\dot{m}_{fuel}$, supplied to the gas turbine cycle is

$$\dot{m}_{fuel} = \frac{\dot{m}_a\,q_{sup}}{LHV} \tag{3}$$

Therefore, the flue gas flow rate is

$$\dot{m}_g = \dot{m}_a + \dot{m}_{fuel} \tag{4}$$

The thermal efficiency of the gas turbine relates to the power output between the heat flow rate supplied in the combustion chamber:

$$\eta_{th,GT} = \frac{\dot{W}_{m,GT}}{\dot{Q}_{sup,CC}} \tag{5}$$

Table 1 shows the pressure, temperature, and mass flow rate of the thermodynamic states of the GT cycle.

Table 1. Thermodynamic states of the gas turbine cycle.

State	Pressure (bar)	Temperature (°C)	Mass Flow Rate (kg/s)
g_1	P_{atm}	$T_{g1} = T_{amb}$	$\dot{m}_a$
g_2	$P_{g_1}\,\pi_C$	$T_{g2} = T_{g1}\left[1+\frac{1}{\eta_{IC}}\left(\pi_C^{x_a}-1\right)\right]$	$\dot{m}_a$
g_3	$P_{g_2}(1-\Delta P_{CC})$	T_{g3}	$\dot{m}_g = \dot{m}_a + \dot{m}_{fuel}$
g_4	$P_{g_1}(1+\Delta P_{GT})$	$T_{g4} = T_{g3}\left\langle 1-\eta_{IGT}\left\{\left[1-\frac{(1+\Delta P_{GT})}{\pi_C(1-\Delta P_{CC})}\right]^{x_g}\right\}\right\rangle$	$\dot{m}_g$

Note that the enthalpy per unit mass of air and combustion gases are determined as follows:

$$h_{g_j} = c_{p,i}\left(T_{g_j} - T_{ref}\right) \tag{6}$$

and the entropy per unit mass of air and combustion gases is

$$s_{g_j} = s_0 + c_{p,i}\ln\left(\frac{T_{g_j}}{T_0}\right) - R_i\ln\left(\frac{P_{g_j}}{P_0}\right) \tag{7}$$

where *j* has the values of the thermodynamic states of the exhaust gases from the inlet of the gas turbine and to the outlet of the heat recovery boiler of the ORC configuration type.

2.3.2. Steam Cycle

The work output in the steam cycle is the difference between the work produced by the turbine and the work supplied to the condensate pump; that is, the following holds:

$$w_{m,SC} = (h_{s1} - h_{s2}) - (h_{s4} - h_{s3}) \tag{8}$$

The heat supplied per unit mass of the exhaust gases to the working fluid in the economizer, evaporator, and superheater of the HRSG is expressed as follows:

$$q_{sup,SC} = (h_{s1} - h_{s4}) \tag{9}$$

The mass flow rate and temperature of the gas turbine exhaust gases are the input data for the energy analysis of the steam cycle. This flow of residual thermal energy is used in the HRSG to generate a mass flow of steam, which expands in the turbine to generate additional power. Therefore, the mass flow rate of steam as a function of the Pinch Point temperature difference is

$$\dot{m}_s = \frac{\dot{m}_g c_{p_g} \left[T_{g4} - (T_{s5} + \Delta T_{PP,SC}) \right]}{(h_{s1} - h_{s5})} \tag{10}$$

The thermal efficiency of the steam cycle relates to the amount of work output produced between the heat supplied by the exhaust gases in the HRSG:

$$\eta_{th,SC} = \frac{w_{m,SC}}{q_{sup,SC}} \tag{11}$$

The power output by the steam cycle is the product of the steam flow rate and the work output produced:

$$\dot{W}_{m,SC} = \dot{m}_s \, w_{m,SC} \tag{12}$$

2.3.3. Organic Rankine Cycle *S-ORC*, *SP-ORC* y *UC-ORC*

In this work, we propose to integrating the configuration of an ORC to take advantage of the amount of residual thermal energy of the exhaust gases that come from the HRSG of the steam cycle. Table 2 shows the main performance parameters with which the *S-ORC*, *SP-ORC*, and *UC-ORC* configurations are evaluated.

Table 2. Performance parameters of the configurations *S-ORC*, *SP-ORC* y *UC-ORC*.

Work output			
$w_{m,l} = (h_{o1} - h_{o2}) - (h_{o4} - h_{o3})$ where l = S-ORC, SP-ORC		$w_{m,UC\text{-}ORC} = (h_{o1} - h_{o2}) + (h_{o3} - h_{o4}) - (h_{o6} - h_{o5})$	
Heat supplied			
$q_{sup,l} = (h_{o1} - h_{o4})$ where l = S-ORC, SP-ORC		$q_{sup,UC\text{-}ORC} = (h_{o1} - h_{o6}) + (h_{o3} - h_{o2})$	
Thermal efficiency			
$\eta_{th,l} = \frac{w_{m,l}}{q_{sup,l}}$ where l = S-ORC, SP-ORC y UC-ORC			
Organic mass flow rate			
$\dot{m}_{org,S\text{-}ORC} = \frac{\dot{m}_g c_{p_g} \left[T_{g7} - (T_{o5} + \Delta T_{PP,S\text{-}ORC}) \right]}{(h_{o1} - h_{o5})}$	$\dot{m}_{org,SP\text{-}ORC} = \frac{\dot{m}_g c_{p_g} \left(T_{g7} - T_{g8} \right)}{q_{sup,SP\text{-}ORC}}$	$\dot{m}_{org,UC\text{-}ORC} = \frac{\dot{m}_g c_{p_g} \left(T_{g7} - T_{g8} \right)}{q_{sup,UC\text{-}ORC}}$	
Power output			
$\dot{W}_{m,l} = \dot{m}_{org} \, w_{m,l}$ where l = S-ORC, SP-ORC			

2.3.4. Power Output Trigeneration Cycle

The total power output by the trigeneration system is the sum of the power output by the gas turbine system, steam cycle, and the power output of the *S-ORC, SP-ORC,* and *UC-ORC* configurations; that is, the following holds:

$$\dot{W}_{m,tri} = \dot{W}_{m,GT} + \dot{W}_{m,SC} + \dot{W}_{m,l} \quad \text{where: } l = \text{S-ORC, SP-ORC y UC-ORC} \tag{13}$$

The thermal efficiency of the trigeneration power system is the ratio of the total power output to the heat flux supplied in the combustion chamber:

$$\eta_{th,tri} = \frac{\dot{W}_{m,tri}}{\dot{Q}_{sup,CC}} \tag{14}$$

2.4. Exergetic Analysis

The exergy of a material stream is the maximum amount of available work that can be obtained from said stream by taking it from the conditions of the initial state to the conditions of the dead state. The exergetic analysis carried out in this work only considers the physical exergy in the gas turbine system, steam cycle, and the *S-ORC, SP-ORC,* and *UC-ORC* configurations.

The physical exergy flow rate for the steam cycle and ORC configurations is as follows:

$$\dot{E}_{ki}^{ph} = \dot{m}_k[(h_i - h_0) - T_0(s_i - s_0)] \text{ where } k = s, org \ i = 1, \ldots, 8 \tag{15}$$

The physical exergy flow rate of the gas turbine cycle considering air and exhaust gases as perfect gas is expressed as follows:

$$\dot{E}_k^{ph} = \dot{m}_k c_{p_k}\left[(T_{gi} - T_0) - T_0 \ln\frac{T_{gi}}{T_0} + T_0\left(\frac{\gamma_k - 1}{\gamma_k}\right)ln\frac{P_{gi}}{P_0}\right] \text{ en donde } k = a, eg \ i = 1, \ldots, 10 \tag{16}$$

The flow of irreversibilities generated by the equipment processes that make up the gas turbine cycle, steam cycle, and ORC configurations are determined through an exergy balance. Table 3 shows the exergy balances of the different equipment that make up the trigeneration power system.

$$\dot{I}_i = \sum \dot{E}_{in_i} - \sum \dot{E}_{out_i} \tag{17}$$

The exergetic efficiency of a system can be defined as the relationship between the useful product obtained from the power system and the resource supplied. The exergetic efficiency of the gas turbine system is

$$\eta_{exer,GT} = \frac{\dot{W}_{m,GT}}{\dot{E}_{fuel}} \tag{18}$$

Likewise, the exergy efficiency of the steam cycle is

$$\eta_{exer,SC} = \frac{\dot{W}_{m,SC}}{\Delta\dot{E}_{g4-g7}} \tag{19}$$

The exergetic efficiency of the *S-ORC, SP-ORC,* and *UC-ORC* configurations is

$$\eta_{exer,S\text{-}ORC} = \frac{\dot{W}_{m,S\text{-}ORC}}{\Delta\dot{E}_{g7-g10}} \quad \eta_{exer,SP\text{-}ORC} = \frac{\dot{W}_{m,SP\text{-}ORC}}{\Delta\dot{E}_{g7-g8}} \quad \eta_{exer,UC\text{-}ORC} = \frac{\dot{W}_{m,UC\text{-}ORC}}{\Delta\dot{E}_{g7-g8}} \tag{20}$$

Finally, the exergetic efficiency of the trigeneration power system is

$$\eta_{exer,tri} = \frac{\dot{W}_{m,tri}}{\dot{E}_{fuel}} \tag{21}$$

where the exergy flow of the fuel supplied into the combustion chamber of the gas turbine system is

$$\dot{E}_{fuel} = \dot{m}_{fuel}LHV\left(1 - \frac{T_0}{T_{af}}\right) \tag{22}$$

Table 3. Exergy balance of the equipment that makes up the trigeneration power system.

Equipment	$\dot{I}_i = \sum \dot{E}_{in_i} - \sum \dot{E}_{out_i}$	Equipment	$\dot{I}_i = \sum \dot{E}_{in_i} - \sum \dot{E}_{out_i}$
	GT		*S-ORC (cont.)*
CC	$\dot{E}_{fuel} + \left(\dot{E}_{g2} - \dot{E}_{g3}\right)$	T_{ORC}	$\left(\dot{E}_{o1} - \dot{E}_{o2}\right) - \left(\dot{E}^{\dot{W}_{m,ORC}} + \dot{E}^{\dot{W}_P}\right)$
C	$\dot{E}^{\dot{W}_C} + \left(\dot{E}_{g1} - \dot{E}_{g2}\right)$	P	$\dot{E}^{\dot{W}_{P2}} + \left(\dot{E}_{o3} - \dot{E}_{o4}\right)$
GT	$\left(\dot{E}_{g3} - \dot{E}_{g4}\right) - \left(\dot{E}^{\dot{W}_{m,GT}} + \dot{E}^{\dot{W}_C}\right)$	COND	$\left(\dot{E}_{o2} - \dot{E}_{o3}\right)$
	SC		*SP-ORC*
SH	$\left(\dot{E}_{g4} - \dot{E}_{g5}\right) + \left(\dot{E}_{s6} - \dot{E}_{s1}\right)$	HRSG	$\left(\dot{E}_{g7} - \dot{E}_{g8}\right) + \left(\dot{E}_{o4} - \dot{E}_{o1}\right)$
EV	$\left(\dot{E}_{g5} - \dot{E}_{g6}\right) + \left(\dot{E}_{s5} - \dot{E}_{s6}\right)$	T_{ORC}	$\left(\dot{E}_{o1} - \dot{E}_{o2}\right) - \dot{E}^{\dot{W}_{T_{ORC}}}$
EC	$\left(\dot{E}_{g6} - \dot{E}_{g7}\right) + \left(\dot{E}_{s4} - \dot{E}_{s5}\right)$	P	$\left(\dot{E}_{o3} - \dot{E}_{o4}\right) + \dot{E}^{\dot{W}_P}$
T_{SC}	$\left(\dot{E}_{s1} - \dot{E}_{s2}\right) - \left(\dot{E}^{\dot{W}_{m,SC}} + \dot{E}^{\dot{W}_P}\right)$	COND	$\left(\dot{E}_{o2} - \dot{E}_{o3}\right)$
P	$\dot{E}^{\dot{W}_{P1}} + \left(\dot{E}_{s3} - \dot{E}_{s4}\right)$		*UC-ORC*
COND	$\dot{E}_{s2} - \dot{E}_{s3}$	HRSG	$\left(\dot{E}_{g7} - \dot{E}_{g8}\right) + \left(\dot{E}_{o6} - \dot{E}_{o1}\right) + \left(\dot{E}_{o2} - \dot{E}_{o3}\right)$
	S-ORC	T_{ORC}	$\left(\dot{E}_{o1} - \dot{E}_{o2}\right) + \left(\dot{E}_{o3} - \dot{E}_{o4}\right) - \dot{E}^{\dot{W}_{HPT}} - \dot{E}^{\dot{W}_{LPT}}$
SH	$\left(\dot{E}_{g7} - \dot{E}_{g8}\right) + \left(\dot{E}_{o6} - \dot{E}_{o1}\right)$	P	$\left(\dot{E}_{o5} - \dot{E}_{o6}\right) + \dot{E}^{\dot{W}_P}$
EV	$\left(\dot{E}_{g8} - \dot{E}_{g9}\right) + \left(\dot{E}_{o5} - \dot{E}_{o6}\right)$	COND	$\left(\dot{E}_{o4} - \dot{E}_{o5}\right)$
EC	$\left(\dot{E}_{g9} - \dot{E}_{g10}\right) + \left(\dot{E}_{o4} - \dot{E}_{o5}\right)$		

2.5. Exergy Optimization

Exergetic optimization of energy generation systems represents a powerful tool aimed at increasing exergetic efficiency, thereby reducing the flow of irreversibilities generated within the system. According to the case study depicted in Figure 1, Figure 2 illustrates the processes of each cycle using a temperature–entropy diagram. In the case of the GT cycle, the exhaust gas flow rate utilized in the HRSG of the steam cycle and in the HRSG of the various ORC configurations is depicted by a decrease in temperature, from T_{g4} to T_{g10} for the steam cycle—*S-ORC*, and from T_{g4} to T_{g8} for the coupling of the steam cycle with the *SP-ORC* and the *UC-ORC*.
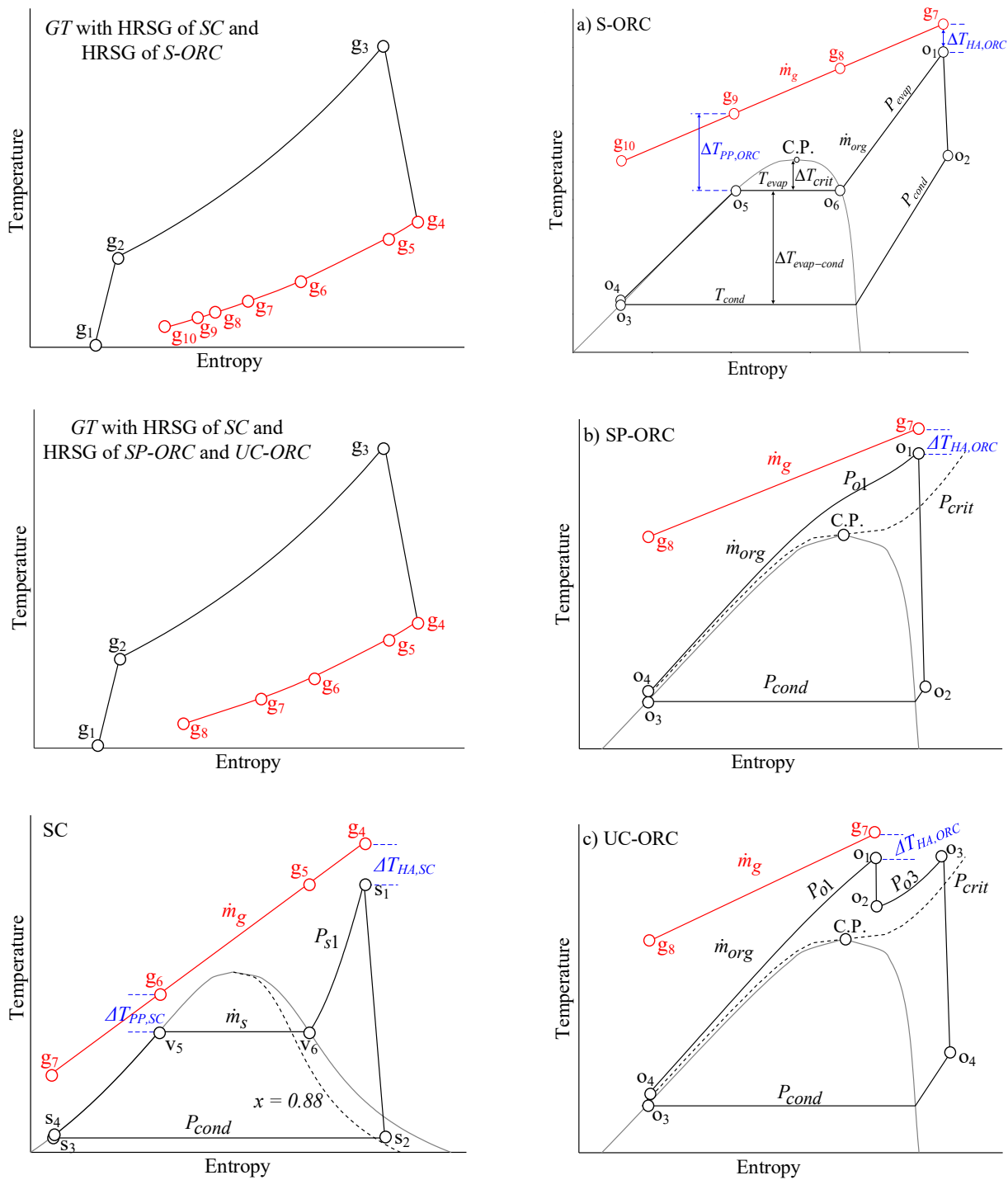
Figure 2. Temperature–entropy diagram of the power trigeneration system TG – CV with (**a**) *S-ORC*, (**b**) *SP-ORC* y, and (**c**) *UC-ORC*.

In accordance with the power trigeneration system, the operating conditions of the gas turbine remain constant and correspond to a specific model type. The flow of residual thermal energy exiting the gas turbine is utilized for generating additional power in both the steam cycle and the *S-ORC*, *SP-ORC*, and *UC-ORC* configurations. Therefore, Figure 2 shows the parameters required to evaluate the performance of both thermodynamic cycles and the limits within which they can operate due to environmental, technological, and fluid working characteristics.

The change In the exergy flow rate of exhaust gases in the HRSG of the steam cycle, $\Delta \dot{E}_{g4\text{-}g7}$, corresponds to the availability of residual thermal energy flow rate utilized for the steam cycle, as depicted in the temperature–entropy diagram in Figure 2. The power output of this cycle is determined by the operating conditions of live steam pressure and temperature, P_{s1} and T_{s1}, condensation temperature, T_{cond}, Pinch Point temperature difference, $\Delta T_{PP,SC}$, and hot approach temperature difference, $\Delta T_{HA,SC}$. These variables represent operating constraints within which the steam cycle can safely operate. From the temperature–entropy diagram of the steam cycle, it is shown that the live steam pressure must be such that the quality of the steam flow at the end of turbine expansion is greater than or equal to 0.88, $x_{s2} \geq 0.88$. Additionally, the live steam temperature for this type of turbine ranges between 450 °C and 500 °C. Regarding the subcritical operation of the *S-ORC*, it is based on the same operating parameters as the steam cycle: Pinch Point temperature difference, $\Delta T_{PP,S\text{-}ORC}$, hot approach temperature difference, $\Delta T_{HA,S\text{-}ORC}$, and the same condensation temperature, T_{cond}. However, in this case, the live steam pressure is determined based on the evaporation temperature, T_{evap}, where this temperature must be higher than the condensation temperature and lower than the critical point temperature, $T_{cond} < T_{evap} < T_{crit}$. When coupling the *SP-ORC* and *UC-ORC* with the steam cycle and gas turbine, the operating conditions are modified according to the live steam pressure and reheating pressure (the latter for *UC-ORC*). Meanwhile, the Pinch Point temperature difference in both cycles ceases to be a decision variable because there is no evaporator in the HRSG. Finally, the exhaust gases utilized in the HRSG of the steam cycle and in the three ORC configurations are released into the environment, where, according to the composition of the fuel type described above, these exhaust gases can be expelled at a minimum temperature of 100 °C.

Therefore, this work proposes an optimization problem that maximizes the overall exergetic efficiency of the power trigeneration system. This can also be analyzed as maximizing the overall power output of the system since the exergy flow rate of the fuel used in the gas turbine combustion chamber is constant, while the variation of the steam cycle and ORC operating parameters is performed to maximize the amount of overall power output. The optimization problem is presented as follows:

$$\underset{x=\{P_{s1},T_{s1},\Delta T_{PP,SC},T_{evap},\Delta T_{HA,ORC},\Delta T_{PP,ORC},P_{o1},P_{reh},T_{cond}\}}{Max} \eta_{exer,tri}$$

$$subject\ to$$

SC

$10 \leq T_{amb} \leq 45$
$T_{g10} \geq 100°C$
$P_{s1} < P_{crit}$
$450 \leq T_{s1} \leq 500$
$\Delta T_{PP,SC} \geq 45$
$x_{s2} \geq 0.88$

S-ORC

$5 \leq \Delta T_{HA,ORC} \leq 10$
$T_{evap} < T_{crit} - \Delta T_{crit}$
$T_{evap} < T_{o1} - \Delta T_{SC}$
$T_{evap} > T_{cond}$
$\Delta T_{PP,ORC} \geq 10$

SP-ORC

$5 \leq \Delta T_{AC,ORC} \leq 10$
$P_{o1} > P_{crit}$
$P_{cond} > P_{trip}$

UC-ORC

$5 \leq \Delta T_{AC,ORC} \leq 10$
$P_{o1} > P_{crit}$
$P_{o1} > P_{reh} > P_{cond}$
$P_{cond} > P_{trip}$

$\sum \dot{E}_{in} - \sum \dot{E}_{out} = \dot{I}_{gen}$
$\boldsymbol{h} = h_{s_i}, h_{o_i} \, i = 1,\dots,8$
$\boldsymbol{s} = s_{s_i}, s_{o_i} \, i = 1,\dots,8$
$\boldsymbol{h} = \boldsymbol{h}(\theta_{j_1}, \theta_{j_2}) \, j = s, o$
$\boldsymbol{s} = \boldsymbol{s}(\beta_{j_1}, \beta_{j_2}) \, j = s, o$

Operating Conditions of the Trigeneration System

The energetic and exergetic analysis of the trigeneration power system is carried out based on the operating conditions of the gas turbine, steam cycle, and the three ORC configurations presented in Tables 4 and 5. The properties of the organic fluids used in the three configurations of the ORC presented in Table 6 are of paramount importance. These properties are essential for evaluating the feasibility of using each organic fluid in the different ORC configurations based on the conditions of the exhaust gas flow from the heat recovery steam generator of the steam cycle.

Table 4. Environmental operating conditions of the gas turbine and steam cycle system.

Ambient		GT		SC
$10\,°C \leq T_{amb} \leq 45\,°C$		π_C, (-)	14	$P_{cond} < P_{s1} < P_{crit}$
P_{atm}, (bar)	0.78	T_{g3}, (°C)	1250	$450\,°C \leq T_{s1} \leq 500\,°C$
		η_{IGT}, (-)	0.9	$\Delta T_{cond} = 10\,°C$
		η_{IC}, (-)	0.88	$\eta_{ISC} = 0.90$
		$\dot{W}_{m,GT}$, (kW)	150,000	$\eta_{IP} = 0.85$
		$\dot{m}_g$, (kg$_g$/s)	351.05	$\Delta T_{HA} \geq 35\,°C$
		T_{g4}, (°C)	655.70	$\Delta T_{PP} \geq 45\,°C$
		ΔP_{CC} (-)	0.04	
		ΔP_{GT} (-)	0.04	

Table 5. Configuration operating conditions S-ORC, SP-ORC y UC-ORC.

S-ORC	SP-ORC	UC-ORC
$T_{crit} > T_{evap} > T_{cond}$		$P_{o1} > P_{crit}$
$\Delta T_{PP} \geq 10\,°C$	$P_{o1} > P_{crit}$	$P_{crit} < P_{o2} < P_{o1}$
	$\Delta T_{cond} = 10\,°C$	
	$\eta_{IORC} = 0.90$	
	$\eta_{IP} = 0.85$	
	$\Delta T_{AC} \geq 5\,°C$	
$T_{g10} \geq 100\,°C$	$T_{g8} \geq 100\,°C$	

Table 6. Properties of organic fluids.

Organic Fluid	T_{crit} (°C)	P_{crit} (bar)	PM (kg/kmol)	GWP	ODP
R1234yf	94.70	33.82	114.04	<1	0
R290	96.74	42.51	44.10	3	0
R134a	101.06	40.59	102.03	1430	0
R1234ze	109.36	36.35	114.04	<1	0
R152a	113.26	45.17	66.05	124	0
R600a	134.66	36.29	58.12	3	0
R245fa	154.01	36.51	134.05	950	0
R123	183.68	36.62	152.93	79	0.01

3. Results and Discussion

The analysis of the results presented below is based on determining the possible operating zones of the steam cycle and the three ORC configurations that have the greatest power generation and exergetic efficiency through a parametric analysis. These zones are limited to the safe operation of both cycles presented in Section Operating Conditions of the Trigeneration System. It begins with the energy analysis of the steam cycle, where the environmental temperature conditions and the operating variables of the cycle are varied. Subsequently, based on a constant operating condition of the steam cycle, a parametric analysis is performed on the three ORC configurations using the eight organic fluids presented in Table 6.

3.1. Energetic and Exergetic Analysis

3.1.1. Steam Cycle

The residual thermal energy flow rate from the HRSG of the steam cycle is utilized to generate steam by varying the live steam pressure and condensation pressure. The inlet pressure to the turbine, P_{s1}, can be increased until the steam quality at the end of the expansion, x_{s2}, is greater than or equal to 0.88. The pressure at the end of the expansion, which is the condensation pressure, P_{cond}, is dependent on the ambient temperature.

Therefore, Figure 3 illustrates the behavior of the power output variation of the steam cycle and steam quality at the outlet of the steam turbine and the influence of ambient temperature variation on live steam pressure and condensation temperature. For different ambient temperatures and operating conditions, higher live steam pressure and temperature result in greater power generation by the steam cycle. However, at the minimum ambient temperature, $T_{amb} = 10\ °C$, the condition for maximum power generation results in a steam quality below the technical limit of 0.88. Therefore, it is necessary to reduce the live steam pressure to increase this parameter [17]. Consequently, only the steam cycle with the minimum temperature and different sets of live steam pressure and temperature possibilities are analyzed.
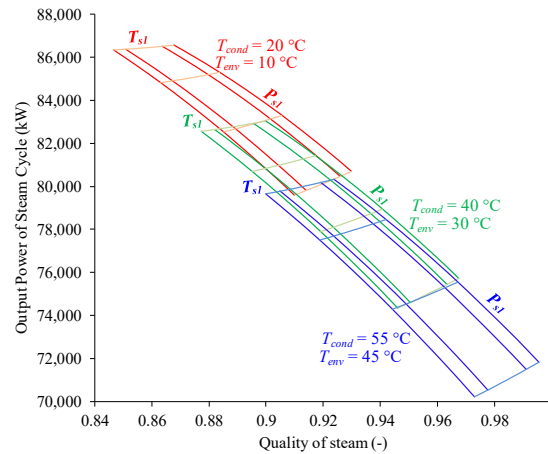

Figure 3. Steam cycle power and steam quality at different condensation temperatures.

On the other hand, according to Equation (10), steam flow rate generation depends on the Pinch Point temperature difference and live steam temperature and pressure. Figure 4 shows the variation in power output by the steam cycle as a function of live steam pressure and temperature, as well as the Pinch Point temperature difference. It is evident that increasing the power output by the steam cycle is due to the increase in live steam pressure, and higher power output occurs with lower Pinch Point temperature differences because of increased steam flow rate in the HRSG.
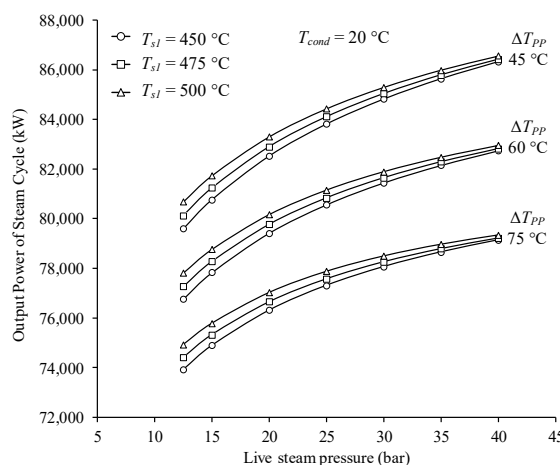

Figure 4. Steam cycle power at different live steam pressures and different Pinch Point temperature differences.

Figure 5 shows the behavior of power generated by the steam cycle and steam quality as a function of live steam pressure and temperature variation. The Figure shows more pronounced increases in power output for pressures from 10 to 25 bar when increasing

live steam temperature from 450 °C to 500 °C. In this range, the steam cycle can operate safely under live steam temperatures and pressures between 10 bar and slightly above 20 bar. However, safe operation of the steam cycle at higher pressures is only possible at a temperature of 500 °C and pressures slightly above 30 bar, generating powers exceeding 85,000 kW. Under this scenario, the steam cycle can achieve a thermal efficiency of up to 35.7%, as shown in Figure 6.
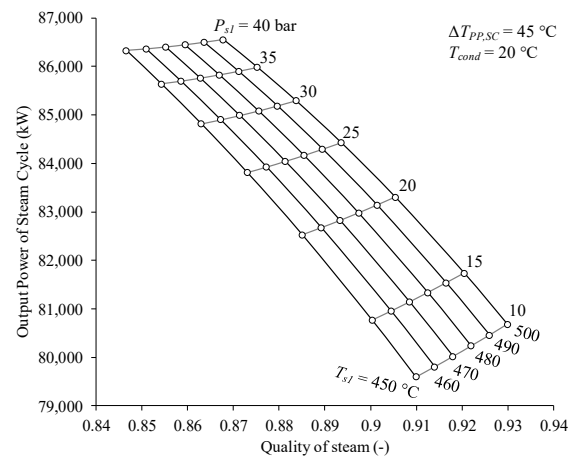

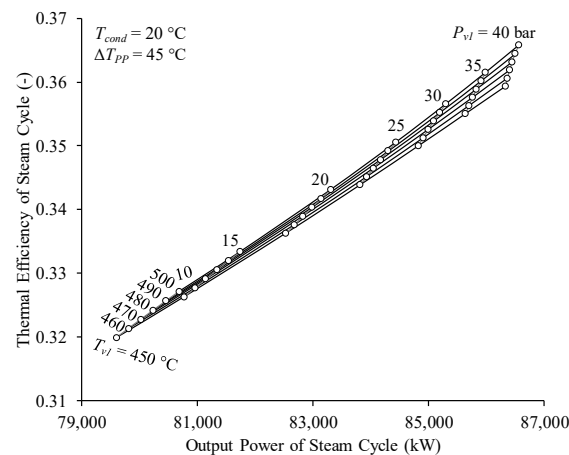**Figure 5.** Steam cycle power and steam quality.

Figure 6. Power and thermal efficiency of the steam cycle.

Based on the above, the chosen operating condition for the steam cycle, balancing safe operation and proximity to maximum power output, is a live steam pressure and temperature of 30 bar and 500 °C, respectively, with a condensation temperature of 20 °C and a Pinch Point temperature difference of 45 °C. From these steam cycle conditions, the exhaust gas temperature at the outlet of the HRSGS economizer is determined. These data are crucial for determining the residual thermal energy flow to be utilized in the ORC HRSG to generate a steam flow rate from the eight proposed organic fluids.

3.1.2. Organic Rankine Cycle

In this section, eight organic fluids are evaluated in the three ORC configurations shown in Figure 1 with the aim of analyzing their behavior in power generation and the required refrigerant mass flow rate as a function of evaporator pressure variation. According to the operating conditions adopted for the steam cycle, the residual thermal energy flow rate utilized in the ORC HRSG of the three configurations has a gas flow rate

of 350 kg_g/s and a temperature of 137.17 °C. Thus, based on the minimum temperature at which exhaust gases can exit the chimney, a thermal head of only 37.17 °C is obtained.

Figure 7 shows the variation in power output and organic flow rate as a function of evaporator pressure for the *S-ORC* configuration. According to the operating conditions shown in Table 5, the TIT for the *S-ORC*, T_{o1}, is 132.17 °C, and in this case, the critical temperature of the R1234yf, R-290, R134a, R1234ze, and R152a fluids is lower than the turbine inlet temperature. Thus, the evaporator pressure variation is performed from a pressure greater than the condensation pressure and less than the critical pressure, $P_{cond} < P_{evap} < P_{crit}$. The use of these working fluids in the *S-ORC* configuration shows an increase in power generation and organic flow with increasing evaporator pressure, with the highest power generated and the highest organic flow occurring at the highest evaporator pressure. The highest power output of 2826.62 kW was generated using R152a, and it also had the second lowest organic flow rate at 48.12 kg/s. On the other hand, the critical temperature of the R-600a, R245fa, and R123 organic fluids exceeds the temperature To1, and in this case, the maximum evaporation temperature for thermodynamic study must be lower than the TIT minus a superheater temperature difference, $T_{evap} = T_{o1} - \Delta T_{SH}$. In the case of using R-600a, R245fa, and R123 in the *S-ORC*, it is observed that maximum power output is generated at one evaporator pressure, followed by a decrease. This behavior occurs because the minimum value of the Pinch Point temperature difference (see Table 5) is reached for evaporator pressures above the maximum power condition. Therefore, increasing the evaporator pressure with a constant Pinch Point temperature difference results in a decrease in both organic flow rate and power output. Similarly, the powers achieved using R245fa and R123 are similar at 2696.39 kW and 2685.01 kW, respectively, and the required mass flows to generate these powers fall within the range of 60 kg/s to 70 kg/s. Regarding the use of R-600a in the *S-ORC*, it presents a power of 2630 kW with the lowest organic flow rate of 33.90 kg/s compared to the eight fluids analyzed in this study.
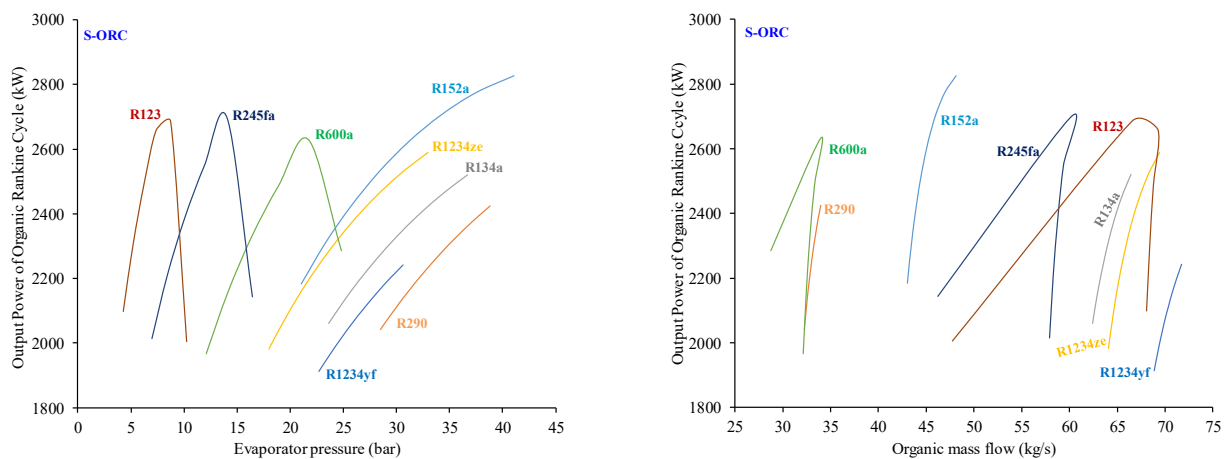

Figure 7. Power output and organic flow rate for the *S-ORC* configuration.

According to the conditions of the residual thermal resource from the HRSG of the *S-ORC*, the use of R1234yf, R-290, R134a, R1234ze, and R152a showed that maximum power output was achieved with an evaporator pressure close to the critical pressure of each fluid. The power output curve consistently exhibits an upward trend. For this reason, the use of these fluids is analyzed under turbine inlet pressures exceeding the critical pressure. Subsequently, the analysis of power generation behavior and required organic flow in the *SP-ORC* and *UC-ORC* configurations shown in Figure 8 is presented. In contrast to the *S-ORC*, the *SP-ORC* reveals a turbine inlet pressure condition where power output reaches its maximum with the use of the five available organic fluids. The highest power output is achieved when using R152a, with a value close to 2900 kW, followed by R1234ze, R134a, and R290, all with values close to 2700 kW. In the case of R1234yf, a slightly higher

power of over 2600 kW is generated. Increasing the pressure above the critical pressure of each organic fluid indicates that, with higher power generation, the difference between the turbine inlet pressure and the critical pressure decreases. Taking the case of R152a, where the highest power is achieved, the pressure difference is over 4 bar. Conversely, when using R1234yf, which generates the lowest amount of power, the largest pressure difference is observed, around 17 bar. The behavior of the required organic flow to achieve these powers reveals that both R290 and R152a require the lowest quantities, with flows of 38 kg/s and 52 kg/s, respectively. In contrast, the use of organic fluids R1234yf, R134a, and R1234ze involves flow quantities ranging from approximately 70 kg/s to 85 kg/s.
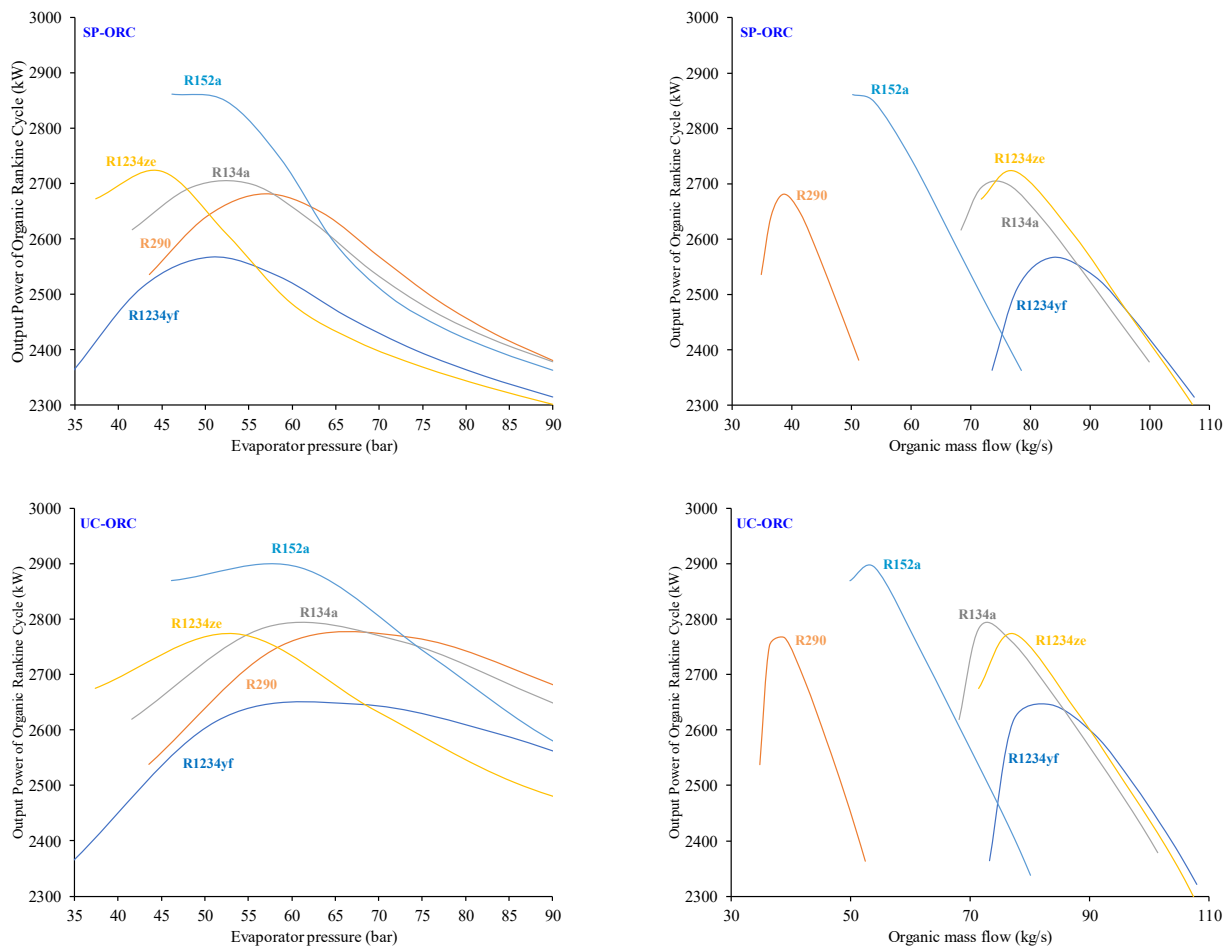

Figure 8. Power and organic flow for the configurations of the *SP-ORC* y *UC-ORC*.

On the other hand, the *UC-ORC* configuration shows the potential to increase cycle power output by increasing the high-pressure turbine inlet pressure, adding a low-pressure turbine, and a reheater. Similar to the *SP-ORC*, the *UC-ORC* exhibits a specific vapor pressure region where maximum power output is achieved using fluids R1234yf, R-290, R134a, R1234ze, and R152a. In this scenario, the region surrounding the maximum power condition presents a wider range of turbine inlet pressures. In other words, it is possible to operate very close to the maximum generated power condition but with a lower turbine inlet pressure. The increase in power generation of the *UC-ORC*, compared to the *SP-ORC*, is notably more significant when using R-290 and R134a with 85.40 kW and 87.28 kW, respectively. Additionally, the use of organic fluid R152a continues to generate the highest power among the five fluids, exceeding 2900 kW. On the other hand, the required organic flow to achieve the powers in the *UC-ORC* exhibits behavior similar to the values recorded in the *SP-ORC*. However, a decrease of less than 1 kg/s in mass flow is shown. This variation is attributed to the increase in the work output resulting from the increase in turbine inlet

pressure and the incorporation of a low-pressure turbine. The power trigeneration system proposed in this study aims to determine the operating conditions that allow maximizing the utilization of residual thermal energy from gas turbine exhaust. The exergetic efficiency behavior is presented using the organic fluids R1234yf, R-290, R134a, R1234ze, R152a, R600a, R245fa, and R123 for the *S-ORC*, *SP-ORC*, and *UC-ORC*.

Figure 9 exhibits how the exergetic efficiency of the *S-ORC* varies in relation to evaporator pressure using the eight organic fluids. According to the expressions of exergetic efficiency shown in Equation (20), it is noted that the exergy flow rate associated with the residual heat of the exhaust gases remains constant when using R1234yf, R-290, R134a, R1234ze, and R152a. This is because the increase in exergetic efficiency with evaporator pressure follows a similar pattern to that shown in Figure 7. In other words, the operating condition that maximizes power generation also coincides with maximum exergetic efficiency in the *S-ORC*, with values of 47.26%, 51.09%, 53.12%, 54.58%, and 59.57% for the use of fluids R1234yf, R-290, R134a, R1234ze, and R152a, respectively. On the other hand, when using fluids R600a, R245fa, and R123, an increase in exergetic efficiency with evaporator pressure is observed, reaching a maximum. However, this optimal exergetic efficiency condition differs from that which maximizes power generation. Although exergetic efficiency only increases by 1.4% compared to the maximum power condition, power decreases to 344.61 kW with the use of R600a and to 1453.76 kW and 1560.75 kW with R245fa and R123, respectively.
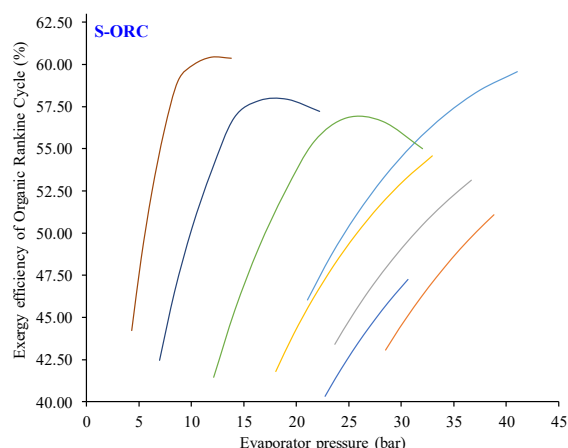

Figure 9. Exergetic efficiency of the *S-ORC* for different evaporator pressures.

Figure 10 shows the behavior of exergetic efficiency concerning the variation of high-pressure turbine inlet pressure for the *SP-ORC* and *UC-ORC*. It is evident that the exergetic efficiency behavior with increasing pressure for the five fluids follows the same pattern as the values shown in Figure 8. Therefore, the *SP-ORC* demonstrates that the zone where maximum exergetic efficiency is found is at a pressure of 46 bar with an efficiency slightly above 0.60, achieved with the use of R152a. In the case of using R290, R134a, and R1234ze, regions of maximum exergetic efficiency are shown between 0.56 and 0.58, and finally, the lowest exergetic efficiency of the *SP-ORC* is observed with the use of R1234yf, which is below 0.54. Similarly, in the *UC-ORC*, it is shown that exergetic efficiencies reflect an increase in using the five organic fluids, with this efficiency increasing to a greater extent with the use of R1234ze, R134a, and R290.

Figure 11 depicts the irreversibility flow of components for the *S-ORC*, *SP-ORC*, and *UC-ORC* under operating conditions close to maximum exergetic efficiency using the eight organic fluids. Comparing the irreversibilities of the components for each organic fluid reveals that R1234yf exhibits the highest irreversibilities, while the use of R152a results in the lowest irreversibility quantities. Across all three ORC configurations, the HRSG components incur the greatest irreversibilities, with the economizer being the primary contributor due to the temperature increase of the organic fluid from condensation temper-

ature to evaporation temperature. Additionally, the condenser ranks second in terms of generating irreversibilities. Finally, the equipment contributing in smaller proportions to exergy destruction includes the pump and the turbine. Increasing the high-pressure turbine inlet pressure results in a reduction in the total irreversibility flow in the *SP-ORC* and *UC-ORC*, leading to an increase in exergetic efficiency. The highest efficiency is observed with the *UC-ORC* using R152a as the working fluid.
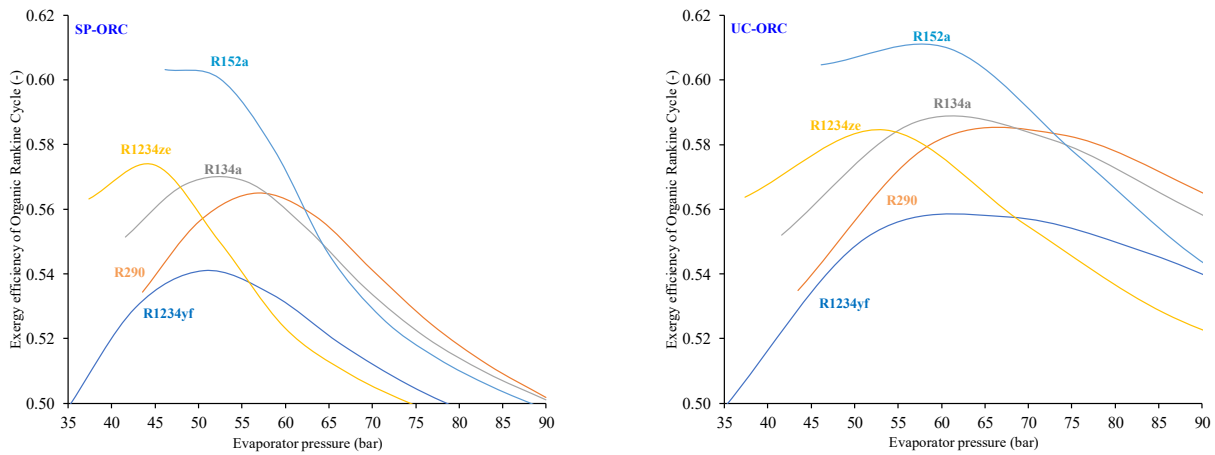
Figure 10. Exergetic efficiency of the *SP-ORC* and *UC-ORC* for different turbine inlet pressures.
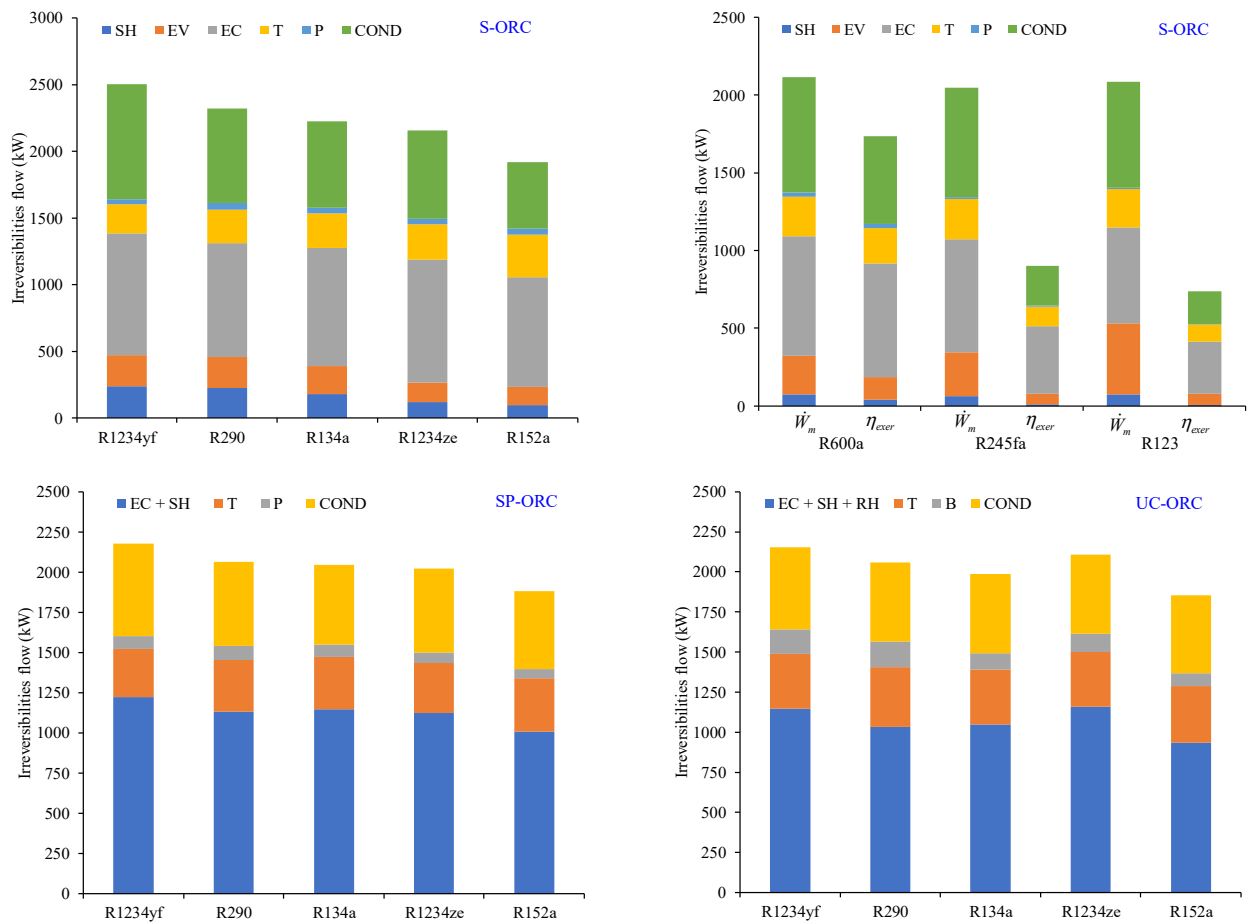
Figure 11. The flow of irreversibilities of the components of the *S-ORC*, *SP-ORC*, and *UC-ORC*.

3.2. Exergy Optimization

Exergetic optimization aims to maximize efficiency, reduce irreversibilities generated within the power trigeneration system components, and maximize energy availability. According to the optimization model proposed in Section 2.5, Tables 7–9 present the operating conditions of decision variables that maximize the exergetic efficiency of the power trigeneration cycle. The maximum exergetic efficiency generally has a value of 55% for the combination of the gas turbine with the steam cycle and the three different ORC configurations. Similarly, the pressure and temperature conditions of live steam, as well as the Pinch Point temperature difference of the steam cycle, remain constant, as does the condensation temperature. In this case, the values obtained in the analysis of Section 3.1.1 turn out to be close to the optimized results shown. Therefore, maximizing exergetic efficiency focuses on comparing the results obtained in the three ORC configurations using the eight organic fluids. The results show that maximizing exergetic efficiency leads to the highest power output. In the case of the *S-ORC*, the use of R152a, R600a, R245fa, and R123 yields the highest powers generated between 2000 kW and 2900 kW. For the *SP-ORC* and *UC-ORC*, the thermodynamic analysis focuses solely on the use of organic fluids R1234yf, R290, R134a, R1234ze, and R152a, with a minimal increase in exergetic efficiency of 0.01% but an increase in power of 447.14, 391.4, 314.08, 216.84, and 164.14 kW, respectively.

Table 7. SC optimization results—*S-ORC*.

	R1234yf	R290	R134a	R1234ze	R152a	R600a	R245fa	R123
P_{s1} (bar)					32.104			
T_{s1} (°C)					500			
$\Delta T_{PP,SC}$ (°C)					45			
T_{evap} (°C)	89.70	91.74	96.06	104.36	108.26	109.31	107.06	104.27
P_{evap} (bar)	30.62	38.84	36.69	32.97	41.05	23.54	14.75	8.63
$\Delta T_{HA,ORC}$ (°C)	7.63	5	5	5	5	10	10	10
$\Delta T_{PP,ORC}$ (°C)	28.57	25.98	22.84	16.75	12.29		10	
T_{cond} (°C)					20			
$\eta_{exer,GT\text{-}SC\text{-}ORC}$ (-)	0.5554	0.5559	0.5561	0.5563	0.5569	0.5566	0.5566	0.5568
$\dot{W}_{m,SC}$ (kW)				85,600.63				
$\dot{W}_{m,S\text{-}ORC}$ (kW)	2321.91	2512.31	2613.26	2683.92	2937.07	2803.89	2836.77	2906.92
$\dot{W}_{m,SC\text{-}S\text{-}ORC}$ (kW)	87,922.49	88,112.89	88,213.84	88,284.50	88,537.65	88,404.47	88,437.35	88,507.50

Table 8. SC optimization results—*SP-ORC*.

	R1234yf	R290	R134a	R1234ze	R152a
P_{s1} (bar)			32.104		
T_{s1} (°C)			500		
$\Delta T_{PP,SC}$ (°C)			45		
P_{o1} (bar)	52.01	58.10	53.28	44.62	48.78
ΔT_{HA} (°C)			5		
T_{cond} (°C)			20		
$\eta_{exer,GT\text{-}SC\text{-}ORC}$ (-)	0.5563	0.5565	0.5566	0.5566	0.5570
$\dot{W}_{m,SC}$ (kW)			85,600.63		
$\dot{W}_{m,SP\text{-}ORC}$ (kW)	2672.40	2792.19	2817.49	2833.87	2982.19
$\dot{W}_{m,SC\text{-}SP\text{-}ORC}$ (kW)	88,273.02	88,392.81	88,418.11	88,434.50	88,582.82

Table 9. SC optimization results—*UC-ORC*.

	R1234yf	R290	R134a	R1234ze	R152a
P_{s1} (bar)			32.104		
T_{s1} (°C)			500		

Table 9. *Cont.*

	R1234yf	R290	R134a	R1234ze	R152a
$\Delta T_{PP,SC}$ (°C)			45		
P_{o1} (bar)	87.37	72.26	64.86	65.19	57.45
P_{o2} (bar)	49.57	52.82	46.97	43.06	45.17
ΔT_{HA} (°C)			5		
T_{cond} (°C)			20		
$\eta_{exer,GT\text{-}SV\text{-}ORC}$ (-)	0.5565	0.5568	0.5569	0.5568	0.5573
$\dot{W}_{m,SC}$ (kW)			85,600.63		
$\dot{W}_{m,UC\text{-}ORC}$ (kW)	2769.05	2903.71	2927.34	2900.76	3101.21
$\dot{W}_{m,SC\text{-}UC\text{-}ORC}$ (kW)	88,369.65	88,504.30	88,527.93	88,501.36	88,701.80

4. Conclusions

This study conducts a thermodynamic analysis aimed at maximizing the exergetic efficiency of a power system comprising a gas turbine cycle, a steam cycle, and three different ORC configurations. The objective is to identify operating conditions that effectively utilize residual gases, initially in the steam cycle's HRSG and subsequently in the *S-ORC*, *SP-ORC*, and *UC-ORC* HRSG, utilizing eight organic fluids. Before optimizing the power trigeneration system, a parametric analysis of the steam cycle and ORC configurations was performed to identify scenarios with the highest exergetic efficiencies and assess the operating conditions that influence decision variables related to the objective function. The optimization problem revealed that the operating conditions for the steam cycle are independent of those optimized for the *S-ORC*, *SP-ORC*, and *UC-ORC*, with a constant live steam pressure and temperature of 32.10 bar and 50 °C, a Pinche Point temperature difference in the evaporator of 45 °C, and a steam cycle power output of 85,600 kW. Thus, coupling the *UC-ORC* with both high and low-temperature cycles emerges as the configuration offering the maximum exergetic efficiency and highest power generation, with 55.73% efficiency and a *UC-ORC* power output of 3101.21 kW, using R152a. Organic fluids R290 and R152a are deemed viable choices due to their low global warming potential, zero ozone depletion potential, and minimal required mass flow rates.

Nomenclature

Abbreviations

C	Compressor
C.P.	Critical Point
CC	Combustion Chamber
COND	Condenser

EC	Economizer
EG	Electrical Generator
EV	Evaporator
GT	Gas Turbine
GWP	Global Warning Potential
HP	High Pressure
HRSG	Heat Recovery Steam Generator
LP	Low Pressure
ODP	Ozone Depletion Potential
ORC	Organic Rankine Cycle
P	Pump
PP	Pinch Point
RH	Reheater
SC	Steam Cycle
SH	Superheater
S-ORC	Simple ORC
SP-ORC	Supercritical ORC
T	Turbine
UC-ORC	Ultracritical ORC

Superscript

| *ph* | physical |

Subscripts

0	dead state
a	air
af	adiabatic flame
amb	ambient
atm	atmospheric
cond	condensation
crit	critial
evap	evaporation
exer	exergetic
fuel	fuel
g	exhaust gases
$g_1,\ldots,g_{10}$	thermodynamic states of gas turbine cycle and HRSG
HA	hot approach
IC	compressor isoentropic efficiency
IGT	gas turbine isoentropic efficiency
in	inlet
m	output
$o_1,\ldots,o_8$	thermodynamic states of organic Rankine cycle
org	organic fluid
out	outlet
p	constant pressure
ref	reference
reh	reheater
$s_1,\ldots,s_8$	thermodynamic states of steam cycle
sup	supplied
th	thermal
tri	trigeneration system

Symbols

c	specific heat	(kJ/kg K)
far	air-fuel ratio	(kg_a/kg_{fuel})
h	enthalpy per unit mass	(kJ/kg)
$\dot{I}$	flow of irreversibilities	(kW)
LHV	low heating value	(kJ/kg_{fuel})
$\dot{m}$	mass flow	(kg/s)
P	pressure	(bar)
$\dot{Q}$	heat flow	(kW)

R	ideal gas constant	(kJ/kg K)
s	entropy per unit mass	(kJ/kg K)
q	heat supplied per unit mass	(kJ/kg)
T	temperature	(°C)
TIT	turbine inlet turbine	(°C)
w	work per unit mass	(kJ/kg)
$\dot{W}$	power	(MW)
x	relation for adiabatic index	(-)
y	relation between temperatures (t_{g3}/t_{g1})	(-)
Greek letters		
$\dot{E}$	exergy flow	(kW)
γ	Adiabatic index	(-)
Δ	increment	(-)
η	efficiency	(-)
π	pressure ratio	(-)

References

1. González, E.V.T.; Hernández, S.C.; Méndez, H.D.L.; Cabañas, F.G.A.; López, J.V.; Leyte, R.L. Comparison of the Parameters of the Exergoeconomic Environmental Analysis of Two Combined Cycles of Three Pressure Levels with and without Postcombustion. *Entropy* **2022**, *24*, 636. [CrossRef] [PubMed]

2. Bakhshmand, S.K.; Saray, R.K.; Bahlouli, K.; Eftekhari, H.; Ebrahimi, A. Exergoeconomic analysis and optimization of a triple-pressure combined cycle plant using evolutionary algorithm. *Energy* **2015**, *93*, 555–567. [CrossRef]

3. Yari, M.; Mehr, A.S.; Zare, V.; Mahmoudi, S.M.S.; Rosen, M.A. Exergoeconomic comparison of TLC (trilateral Rankine cycle), ORC (organic Rankine cycle) and Kalina cycle using a low grade heat source. *Energy* **2015**, *83*, 712–722. [CrossRef]

4. Iglesias Garcia, S.; Ferreiro Garcia, R.; Carbia Carril, J.; Iglesias Garcia, D. A review of thermodynamic cycles used in low temperature recovery systems over the last two years. *Renew. Sustain. Energy Rev.* **2018**, *81*, 760–767. [CrossRef]

5. Vélez, F. Selecting working fluids in an organic Rankine cycle for power generation from low temperature heat sources. *Dyna* **2014**, *81*, 173–180. [CrossRef]

6. Kajurek, J.; Rusowicz, A.; Grzebielec, A.; Bujalski, W.; Futyma, K.; Rudowicz, Z. Selection of refrigerants for a modified organic Rankine cycle. *Energy* **2019**, *168*, 1–8. [CrossRef]

7. Raghulnath, D.; Saravanan, K.; Mahendran, J.; Kumar, M.R.; Lakshmanan, P. Analysis and optimization of organic Rankine cycle for IC engine waste heat recovery system. *Mater. Today Proc.* **2020**, *21*, 30–35. [CrossRef]

8. Mohamed, H.; Bani-Hani, E.; EL Haj Assad, M. Thermal Analysis of Organic Rankine Cycle Using Different Organic Fluids. *Renew. Energy Res. Appl.* **2020**, *1*, 115–121. [CrossRef]

9. Braimakis, K.; Karellas, S. Energetic optimization of regenerative Organic Rankine Cycle (ORC) configurations. *Energy Convers. Manag.* **2018**, *159*, 353–370. [CrossRef]

10. Wang, J.; Yan, Z.; Wang, M.; Ma, S.; Dai, Y. Thermodynamic analysis and optimization of an (organic Rankine cycle) ORC using low grade heat source. *Energy* **2013**, *49*, 356–365. [CrossRef]

11. Mustapić, N.; Brkić, V.; Duić, Ž.; Kralj, T. Thermodynamic Optimization of Advanced Organic Rankine Cycle Configurations for Geothermal Energy Applications. *Energies* **2022**, *15*, 6990. [CrossRef]

12. Mohammadi, A.; Ashouri, M.; Ahmadi, M.H.; Bidi, M.; Sadeghzadeh, M.; Ming, T. Thermoeconomic analysis and multiobjective optimization of a combined gas turbine, steam, and organic Rankine cycle. *Energy Sci. Eng.* **2018**, *6*, 506–522. [CrossRef]

13. Braimakis, K.; Karellas, S. Exergetic optimization of double stage Organic Rankine Cycle (ORC). *Energy* **2018**, *149*, 296–313. [CrossRef]

14. Özdemir Küçük, E.; Kılıç, M. Exergoeconomic analysis and multi-objective optimization of ORC configurations via Taguchi-Grey Relational Methods. *Heliyon* **2023**, *9*, e15007. [CrossRef]

15. Sohrabi, A.; Behbahaninia, A.; Sayadi, S. Thermodynamic optimization and comparative economic analysis of four organic Rankine cycle configurations with a zeotropic mixture. *Energy Convers. Manag.* **2021**, *250*, 114872. [CrossRef]

16. Javanshir, N.; Mahmoudi, S.M.S.; Rosen, M.A. Thermodynamic and Exergoeconomic Analyses of a Novel Combined Cycle Comprised of Vapor-Compression Refrigeration and Organic Rankine Cycles. *Sustainability* **2019**, *11*, 3374. [CrossRef]

17. Şen, G.; Nil, M.; Mamur, H.; Doğan, H.; Karamolla, M.; Karaçor, M.; Kuyucuoğlu, F.; Yörükeren, N.; Bhuiyan, M.R.A. The effect of ambient temperature on electric power generation in natural gas combined cycle power plant—A case study. *Energy Rep.* **2018**, *4*, 682–690. [CrossRef]